

Article

A New Prediction Method for the Complete Characteristic Curves of Centrifugal Pumps

Huokun Li ¹, Hongkang Lin ¹, Wei Huang ^{1,*}, Jiazhen Li ², Min Zeng ³, Jiming Ma ⁴ and Xin Hu ⁵

¹ School of Civil Engineering and Architecture, Nanchang University, Nanchang 330031, China; lihuokun@ncu.edu.cn (H.L.); linhongkang1001@163.com (H.L.)

² State Key Laboratory of Simulation and Regulation of Water Cycle in River Basin, China Institute of Water Resources and Hydropower Research, Beijing 100038, China; neji1989@126.com

³ Department of Hydraulic Engineering, Jiangxi Water Resources Institute, Nanchang 330013, China; jxslxym@163.com

⁴ State Key Laboratory of Hydrosience and Engineering, Tsinghua University, Beijing 100084, China; majiming@mail.tsinghua.edu.cn

⁵ Shanxi Dongshan Water Supply Project Construction Management Co., Ltd., Taiyuan 030000, China; sx_huxin@163.com

* Correspondence: huang-w14@tsinghua.org.cn; Tel.: +86-136-9317-1976

Abstract: Complete pump characteristics (CPCs) are the key for establishing pump boundary conditions and simulating hydraulic transients. However, they are not normally available from manufacturers, making pump station design difficult to carry out. To solve this issue, a novel method considering the inherent operating characteristics of the centrifugal pump is therefore proposed to predict the CPCs. First, depending on the Euler equations and the velocity triangles at the pump impeller, a mathematical model describing the complete characteristics of a centrifugal pump is deduced. Then, based on multiple measured CPCs, the nonlinear functional relationship between the characteristic parameters of the characteristic operating points (COPs) and the specific speed is established. Finally, by combining the mathematical model with the nonlinear relationship, the CPCs for a given specific speed are successfully predicted. A case study shows that the predicted CPCs are basically consistent with the measured data, showing a high prediction accuracy. For a pump-failure water hammer, the simulated results using the predicted CPCs are close to that using the measured data with a small deviation. This method is easy to program and the prediction accuracy meets the requirements for hydraulic transient simulations, providing important data support for engineering design.

Keywords: centrifugal pump; complete characteristic curves; specific speed; hydraulic transient



Citation: Li, H.; Lin, H.; Huang, W.; Li, J.; Zeng, M.; Ma, J.; Hu, X. A New Prediction Method for the Complete Characteristic Curves of Centrifugal Pumps. *Energies* **2021**, *14*, 8580. <https://doi.org/10.3390/en14248580>

Academic Editor: Helena M. Ramos

Received: 22 November 2021

Accepted: 16 December 2021

Published: 20 December 2021

Publisher's Note: MDPI stays neutral with regard to jurisdictional claims in published maps and institutional affiliations.



Copyright: © 2021 by the authors. Licensee MDPI, Basel, Switzerland. This article is an open access article distributed under the terms and conditions of the Creative Commons Attribution (CC BY) license (<https://creativecommons.org/licenses/by/4.0/>).

1. Introduction

Due to its wide range of flow and head, a centrifugal pump is commonly used in the fields of regional water diversion, agricultural irrigation, industrial cooling cycles and urban water supply and drainage [1]. Its hydraulic performance is directly related to the operational safety and benefits of the project [2]. Therefore, obtaining various pump performance parameters is necessary. As the curves showing the relationships among the discharge, head, speed and torque under all possible operating conditions of the pump, the CPCs are a key factor for establishing pump boundary conditions, which provides important data support for the hydraulic transient analysis and the optimum design of the water conveyance system in the pump station [3–5]. However, because the impeller model test is time-consuming and laborious, pump manufacturers generally provide the pump characteristic data in the normal pumping zone but rarely provide the CPCs for all operating zones [6,7]. In addition, engineering practice has shown that in the absence of measured CPCs, simply applying the CPCs with an approximate specific speed may sometimes produce large deviations, which will adversely affect the operational safety of the pumping station project [8,9]. Therefore, obtaining a scientific and reasonable method

to predict the CPCs for an arbitrary specific speed is necessary to accurately simulate the hydraulic transients and guide the design of pump stations.

In 1965, Suter and Marchal [10] first proposed the ‘Suter transformation’, which included the dimensionless head characteristic curve (WH) and torque characteristic curve (WB) under normal and abnormal operating zones. Since then, accurately predicting the WH and WB curves of a centrifugal pump has become a research hotspot. However, due to its complex shape and high nonlinearity, it is difficult to predict the WH and WB curves [11]. To expand the existing data of CPCs, scholars have conducted a series of studies and have achieved fruitful results in the prediction of CPCs. Currently, the main methods used to predict the CPCs can be divided into curve fitting, neural network prediction, and computational fluid dynamics (CFD) prediction.

The curve fitting method constructs a general formula to describe the CPCs at different specific speeds by setting parameters, such as the specific speed and the relative flow angle as independent variables based on existing CPCs data. Izquierdo [12] recommended the use of cubic spline interpolation to fit the CPCs, pointing out that this method can be better utilized for solving the boundary conditions of the pump while ensuring the good fitting effect. Zhu [13] takes the specific speed, relative flow angle and characteristic parameters corresponding to the zero flow condition as independent variables and establishes a new fitting formula for the CPCs by the least squares method. Hu [14] established a three-dimensional Cartesian coordinate system with the relative flow angle, specific speed and WH value (or WB value) as independent variables and interpolated them with a bicubic polynomial to develop a three-dimensional surface visual model for predicting the CPCs. The predicted curves basically match the measured data. Lima [15] constructed an equation for fitting the CPCs in a similar triangular series form while using a particle swarm algorithm to optimize the fitting coefficients, and the predicted CPCs have shown a certain degree of reliability. Wan [16] analyzed the internal relationship between the normal performance curves and the CPCs, successfully inverting the ‘pumping zone’ data in the CPCs, and proved that this inversion method can provide more accurate data for the calculation of the hydraulic transients.

The inherent nonlinearity of the CPCs makes them difficult to predict by traditional system identification methods. A neural network, which is not limited by the nonlinear model and is easy to implement in engineering, shows good adaptability in the prediction. Liu [17] and Lu [18] adopted a three-layer backpropagation (BP) neural network to predict the CPCs for any specific speed based on the three to four measured characteristic data of pumps. Liu [19] used a genetic algorithm (GA) to optimize the number of hidden nodes and the center of the basis function in a radial basis function (RBF) neural network. She proposed a GARBF neural network model for predicting the CPCs, which can take the topology, connection weight, hidden node center and width of the network as a whole for global optimization. To overcome the problems of traditional BP neural networks, which exhibit low learning efficiency and can easily fall into local minima, Han [20] used a combination of the Levenberg–Marquardt (LM) algorithm and a double-hidden layer BP neural network to predict the normal performance curve of pumps, and the results show that the method can reduce the prediction error while shortening the neural network training time. Huang [21] introduced the loss in the inlet pipe, the incidence loss in the pump impeller and the disk friction loss into the BP neural network to further improve the prediction accuracy of the energy performance (i.e., the head, power and efficiency) of centrifugal pumps. Wu [22] built a prediction model of the normal performance curve of an axial flow pump based on an improved RBF neural network, and the prediction results were in good agreement with the experiments.

With the rapid development of modern computer technology, CFD technology has gradually become an effective means to predict the CPCs. CFD technology is used to model the pump in three dimensions, set the operation conditions and calculate the flow field to obtain the simulation results, such as the pump inlet and outlet head, discharge, speed and torque under different operation conditions (including turbine, dissipation, normal pump

and reverse dissipation operation conditions). Finally, the mathematical transformation of these simulation results can realize the prediction of the CPCs. Höller [23] numerically simulated the steady-state and transient conditions of a mixed flow pump with CFD software, proposed a method to obtain the four quadrant characteristic curve of a mixed flow pump, and experimentally verified the accuracy of the method. Gros [24] analyzed and compared the four quadrant characteristic curves of a centrifugal pump obtained by experiments and CFD technology. Wang [25] established a three-dimensional simulation model for a double-suction centrifugal pump by using CFD software and proposed a novel three-dimensional internal characteristics method for determining the WH and WB curves of double-suction centrifugal pumps, which greatly improved the accuracy of the water hammer analysis. Muttalli [26] evaluated the normal performance curve of a centrifugal pump using the ANSYS CFX-14 and discussed the effect of cavitation flow phenomenon on the simulation results. Frosina [27] predicted the inverse characteristic of centrifugal pumps using CFD technology and evaluated the deviation between the performance of pumps-as-turbines obtained by different prediction methods and the experimental results.

Since the existing prediction methods for the CPCs rely mostly on sufficient pump design parameters and the number of training samples or derive the prediction from the perspectives of function fitting and trend prediction, the inherent operating characteristics of the pump are ignored, and the mathematical relationships among parameters, such as head, speed and torque, are not revealed. Therefore, this paper takes several sets of the measured CPCs with different specific speeds as the research object. First, based on the Euler equations and the velocity triangles at the pump impeller when the pump is running at a steady state, a mathematical model describing the complete characteristics of a centrifugal pump is deduced in Section 2. Second, multiple measured CPCs at various specific speeds are transformed to obtain the characteristic parameters corresponding to each COP and the functional relationship between the characteristic parameters and the specific speed is established using a nonlinear regression model in Section 3. Then, this relational model is substituted into the mathematical model describing the CPCs, the undetermined coefficients in the model are solved, and the CPCs for a given specific speed are successfully predicted in Section 4. Finally, a comparison with the measured CPCs and a case study are conducted to validate the proposed prediction method in Section 5. Conclusions are presented in Section 6.

2. Materials and Methods

According to the theorem of moment of momentum, the torque and the theoretical pumping head of a centrifugal pump under steady conditions can be determined by Euler's equation [28,29]:

$$\begin{bmatrix} M \\ H_e \end{bmatrix} = \begin{bmatrix} M \\ \frac{H}{\eta} \end{bmatrix} = \begin{bmatrix} \rho Q \\ \frac{\omega}{g} \end{bmatrix} [V_{2u}r_2 - V_{1u}r_1] \quad (1)$$

where subscripts 1 and 2 represent the impeller inlet and outlet, respectively; M is the shaft torque (N·m); H_e is the theoretical head (m); H is the practical head (m); $\eta = H/(H + KQ^2)$ is the hydraulic efficiency; K is the hydraulic loss coefficient; Q is the discharge (m³/s); ω is the angular velocity of rotation (rad/s); V_u is the peripheral component of the absolute velocity (m/s); r is the impeller radius (m); ρ is the flow density (kg/m³); and g is the gravitational acceleration (m/s²).

Without considering the flow loss at the impeller and assuming that the flow distribution at the impeller inlet or outlet is uniform, the discharge at the impeller inlet can be expressed as [30,31]:

$$Q = V_{1m}A_1 = 2\pi b_1 r_1 V_{1m} \quad (2)$$

where V_{1m} is the meridional flow velocity at the impeller inlet (m/s), A_1 is the section area at the impeller inlet (m²), and b_1 is the section width at the impeller inlet (m).

According to the continuity of water flow, the discharge at the impeller outlet is equal to the flow at the inlet, which is:

$$Q = V_{2m}A_2 = 2\pi b_2 r_2 V_{2m} \tag{3}$$

where V_{2m} is the meridional flow velocity at the impeller outlet (m/s), A_2 is the section area at the impeller outlet (m²), and b_2 is the section width at the impeller outlet (m).

According to the velocity triangle of water flow inside the centrifugal pump impeller shown in Figure 1, V_{1u} and V_{2u} in Equation (1) can be written as [32,33]:

$$V_{1u} = V_{1m} \cot \alpha_1 = \frac{Q \cot \alpha_1}{2\pi b_1 r_1} \tag{4}$$

$$V_{2u} = U_2 - V_{2m} \cot \beta_2 = \omega r_2 - \frac{Q \cot \beta_2}{2\pi b_2 r_2} \tag{5}$$

where U_2 is the peripheral velocity at the impeller outlet (m/s), α_1 is the absolute flow angle at the impeller inlet (°), and β_2 is the relative flow angle at the impeller outlet (°).

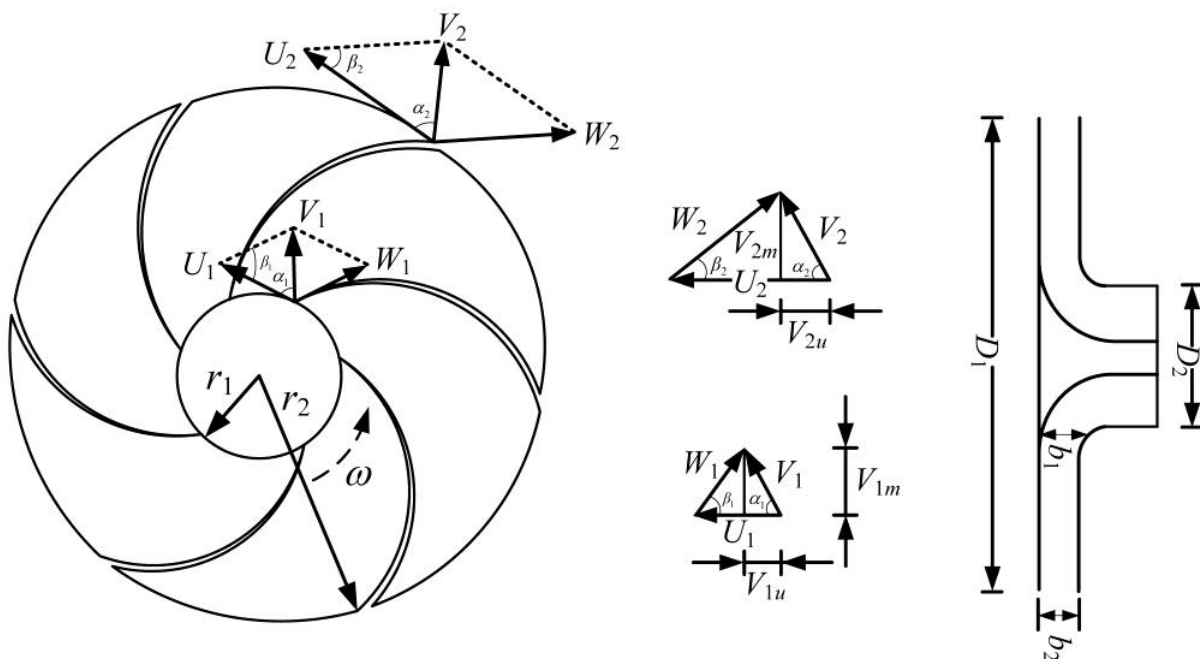


Figure 1. The velocity triangles at the impeller of a centrifugal pump.

Substituting Equations (4) and (5) into Equation (1) yields:

$$\begin{bmatrix} M \\ H_e \end{bmatrix} = \begin{bmatrix} M \\ \frac{H}{\eta} \end{bmatrix} = \begin{bmatrix} \rho Q \\ \frac{\omega}{g} \end{bmatrix} \left[\omega r_2^2 - \left(\frac{\cot \alpha_1}{2\pi b_1} + \frac{\cot \beta_2}{2\pi b_2} \right) Q \right] \tag{6}$$

According to the similarity principle, the following dimensionless similarity relationship exists when a pump has similar working conditions [34]:

$$\frac{q}{n} = Const. \quad \frac{n}{\sqrt{h}} = Const. \quad \frac{q}{\sqrt{h}} = Const. \quad \frac{m}{h} = Const. \tag{7}$$

where $q = Q/Q_r$ is the relative discharge, $h = H/H_r$ is the relative head, $n = N/N_r$ is the relative rotational speed, $m = M/M_r$ is the relative torque, and subscript r represents the rated condition of the pump.

If q/\sqrt{h} and m/h are the abscissas and n/\sqrt{h} is the ordinate, $q/\sqrt{h} - n/\sqrt{h}$ and $m/h - n/\sqrt{h}$ curves can be drawn, respectively, which can reflect the relationship between q , n , h and m of the pump at different speeds. Substituting $q = Q/Q_r$, $n = N/N_r$, $h = H/H_r$, $m = M/M_r$, $\omega = 2\pi N/60$, $\eta = H/(H + KQ^2)$ into Equation (6) and eliminating Q , ω , H and M , the following equations can be deduced:

$$\frac{m}{h} = \lambda_1 \frac{q}{\sqrt{h}} \frac{n}{\sqrt{h}} + \lambda_2 \left(\frac{q}{\sqrt{h}} \right)^2 \quad (8)$$

$$\xi_1 \left(\frac{n}{\sqrt{h}} \right)^2 + \xi_2 \frac{q}{\sqrt{h}} \frac{n}{\sqrt{h}} + \xi_3 \left(\frac{q}{\sqrt{h}} \right)^2 = 1 \quad (9)$$

where $\lambda_1 = \pi \rho r_2^2 Q_r N_r / 30 M_r$, $\lambda_2 = -\rho (\cot \alpha_1 / 2\pi b_1 + \cot \beta_2 / 2\pi b_2) Q_r^2 / M_r$, $\xi_1 = \pi^2 r_2^2 N_r^2 / (900 g H_r)$, $\xi_2 = -\pi (\cot \alpha_1 / 2\pi b_1 + \cot \beta_2 / 2\pi b_2) Q_r N_r / (30 g H_r)$, and $\xi_3 = -K Q_r^2 / H_r$.

The above characterization of the relationship curves among q , h and m under different values of n during steady operating conditions provides the complete characteristics of a centrifugal pump. When a hydraulic transient occurs, the internal flow pattern of the pump is complex, which causes parameters, such as flow rate and torque, to change significantly over time. Analysis of the existing measured CPCs indicates that the corresponding torque is not equal to zero when the discharge is zero. Thus, Equation (9) can be corrected as follows:

$$\frac{m}{h} = \lambda_1 \frac{q}{\sqrt{h}} \frac{n}{\sqrt{h}} + \lambda_2 \left(\frac{q}{\sqrt{h}} \right)^2 + \lambda_3 \quad (10)$$

where λ_3 is the correction factor, which is related to the specific speed of the pump.

Equations (9) and (10) constitute a mathematical model describing the complete characteristics of a centrifugal pump, where Equations (9) and (10) are used to determine the flow characteristics ($q/\sqrt{h} - n/\sqrt{h}$) and the torque characteristics ($m/h - n/\sqrt{h}$), respectively. The shapes of the complete characteristic curves depend on the parameters (such as λ_1 , λ_2 , λ_3 , ξ_1 , ξ_2 , and ξ_3) that are related to the geometric parameters of the impeller and the working condition parameters. However, the above coefficients are unknown before the model test of the pump impeller is carried out [4].

There are two solutions: the direct method and indirect method, and flow charts for these two methods are shown in Figure 2. The direct method refers to the statistics of the geometric parameters and working condition parameters of pumps with different specific speeds, including the impeller diameter, the section width at the impeller inlet and outlet, the absolute flow angle and the relative flow angle. Then, the relationship between these parameters and the specific speeds can be determined by regression analysis; thus, the values of λ_1 , λ_2 , λ_3 , ξ_1 , ξ_2 , and ξ_3 of the pump at a given specific speed can be directly determined according to the definitions of these parameters. Generally, the statistics of working condition parameters in the direct method are more difficult. Therefore, the indirect method can be used.

Since the CPCs are comprised of a series of curves reflecting the relationship between q , n , h and m , the $q/\sqrt{h} - n/\sqrt{h}$ relation curve and $m/h - n/\sqrt{h}$ relation curve can be obtained by mathematical transformation. Then, several COPs are collected on the complete characteristic curves of centrifugal pumps with different specific speeds and the regression model is developed for their dimensionless characteristic parameters (q/\sqrt{h} , n/\sqrt{h} and m/h) as functions of specific speed. When the specific speed is given, the characteristic parameters corresponding to these COPs on the CPCs can be approximately determined according to the regression model. Thus, the values of λ_1 , λ_2 , λ_3 , ξ_1 , ξ_2 , and ξ_3 can be indirectly determined by substituting the values of q/\sqrt{h} , n/\sqrt{h} and m/h of COPs into Equations (9) and (10). Considering that both Equations (9) and (10) have only three undetermined coefficients, the values of these coefficients in theory can be determined if the dimensionless characteristic parameters (q/\sqrt{h} , n/\sqrt{h} and m/h) of three COPs in the corresponding operating region are known. Since the characteristic parameters of the measured COPs are easier to obtain, the indirect method is applied to predict the complete characteristics of a centrifugal pump.

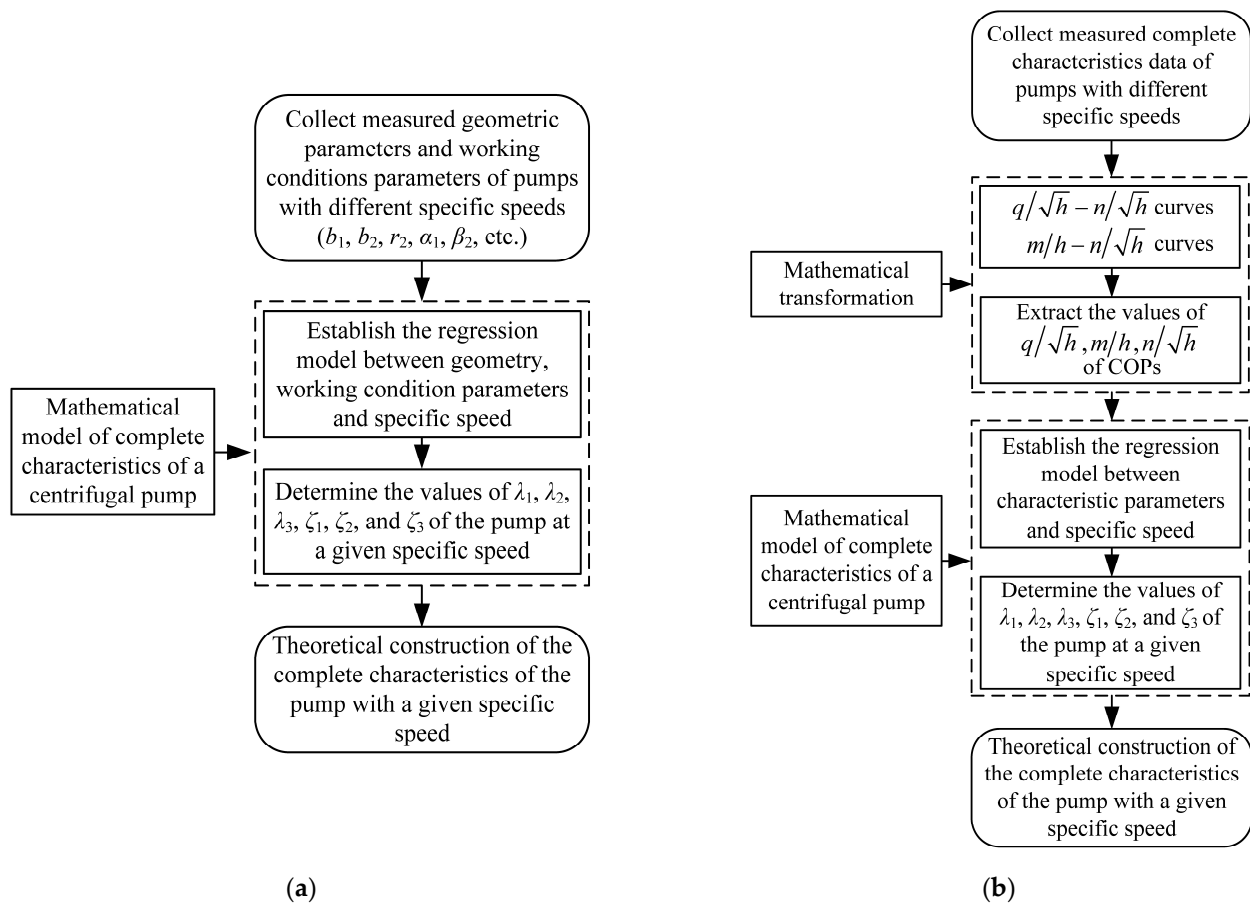


Figure 2. Flow charts of two methods: (a) direct method; (b) indirect method.

3. Suter Transformation and COP Analysis of Complete Characteristic Curves

3.1. Suter Transformation

Because q , n , h and m may change signs and pass through zero during a transient process, it is not convenient to use the $q/\sqrt{h} - n/\sqrt{h}$ relation curve and $m/h - n/\sqrt{h}$ relation curve for the hydraulic transient simulation of a pump station directly. Therefore, Suter and Marchal [10] proposed the following mathematical transformations based on the dimensionless similar characteristics of pumps:

$$WH(x) = \frac{h}{q^2 + n^2} \quad (11)$$

$$WB(x) = \frac{m}{q^2 + n^2} \quad (12)$$

$$x = \begin{cases} \arctan\left(\frac{q}{n}\right), & n < 0, q \leq 0 \\ \pi + \arctan\left(\frac{q}{n}\right), & n \geq 0 \\ 2\pi + \arctan\left(\frac{q}{n}\right), & n < 0, q \geq 0 \end{cases} \quad (13)$$

where x represents the instantaneous position of pump operation and WH and WB represent the head characteristics and torque characteristics of the pump, respectively.

Equations (11) and (12) are valid for any real numbers of n and q except that n and q are equal to zero simultaneously when the pump is shut down. As shown in Figure 3, according to the positive and negative relationship between n and q , the entire operating conditions of the pump can be divided into the turbine zone ($q \leq 0, n < 0$, first quadrant), dissipation zone ($q < 0, n \geq 0$, second quadrant), normal pump zone ($q > 0, n \geq 0$, third quadrant) and reverse dissipation zone ($q > 0, n < 0$, fourth quadrant) [35]. When the pump is stopped in the case of an accident, water does not usually flow out of the pump while the

pump is reversed. In other words, the operating condition trajectory of the pump generally does not enter the reverse dissipation zone (shadow area in Figure 3), so the data for the first to third quadrants in the CPCs can meet the calculation requirements of the hydraulic transients [36,37].

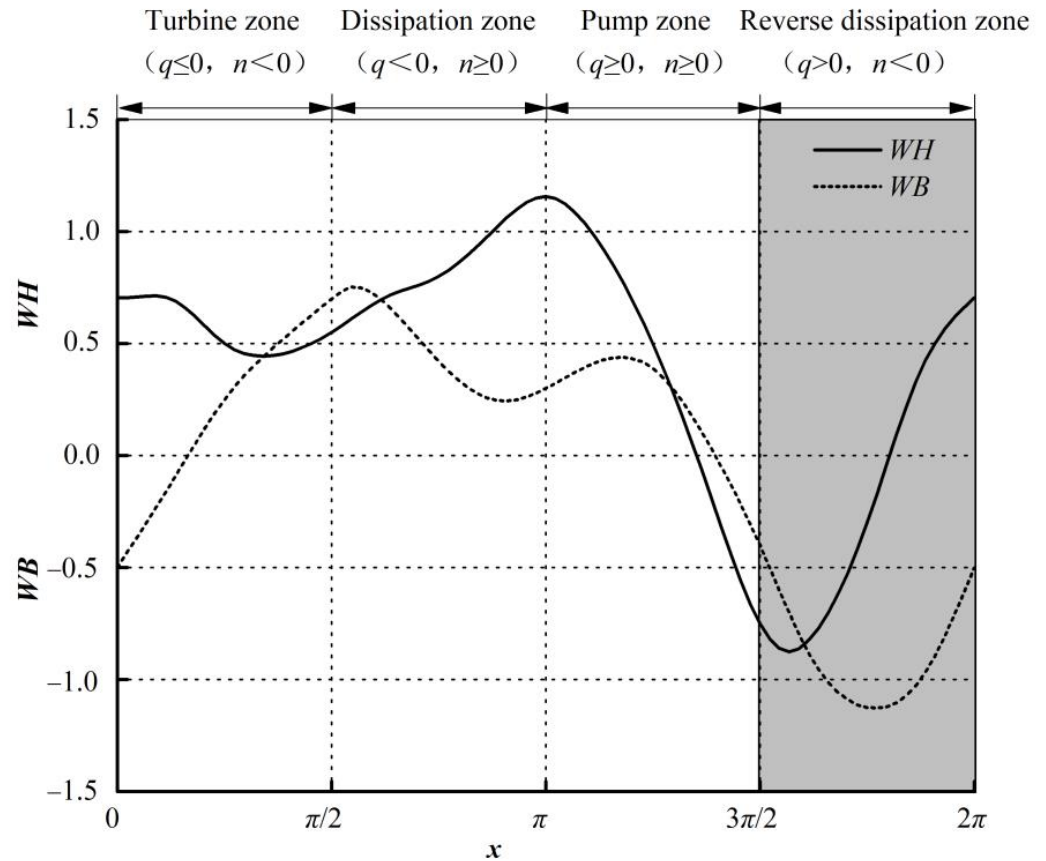


Figure 3. Complete characteristic curves and operation zones of the pump.

To use the CPCs for the numerical simulation, the curves in Figure 2 will be stored as data arrays $(x_i, WH(x_i), WB(x_i))$ in a computer. Based on Equation (13), the value of q/n can be determined as follows:

$$\frac{q}{n}(x_i) = \begin{cases} \tan x_i, x_i \in [0, \frac{\pi}{2}) \\ \tan(x_i - \pi), x_i \in (\frac{\pi}{2}, \frac{3\pi}{2}) \end{cases} \tag{14}$$

Transforming the Equation (11) yields:

$$\frac{n^2}{h}(x_i) = \frac{1}{WH(x_i) [1 + (\frac{q}{n}(x_i))^2]} \tag{15}$$

$$\frac{q^2}{h}(x_i) = \frac{n^2}{h}(x_i) \left(\frac{q}{n}(x_i)\right)^2 \tag{16}$$

Combining Equations (14)–(16), and according to the positive and negative relationship of n and q corresponding to the pump operation zones where x_i is located, the values of n/\sqrt{h} and q/\sqrt{h} corresponding to any x_i can be given as follows:

$$\frac{n}{\sqrt{h}}(x_i) = \begin{cases} -\frac{1}{\sqrt{WH(x_i) [1 + (\frac{q}{n}(x_i))^2]}}, x_i \in [0, \frac{\pi}{2}) \\ 0, x_i = \frac{\pi}{2} \\ \frac{1}{\sqrt{WH(x_i) [1 + (\frac{q}{n}(x_i))^2]}}, x_i \in (\frac{\pi}{2}, x_1] \end{cases} \tag{17}$$

where x_1 is the x_i value corresponding to $WH > 0$ in the range of $(\frac{\pi}{2}, \frac{3\pi}{2}]$.

$$\frac{q}{\sqrt{h}}(x_i) = \begin{cases} \frac{n}{\sqrt{h}}(x_i)\frac{q}{n}(x_i), & x_i \in [0, \frac{\pi}{2}) \cup (\frac{\pi}{2}, x_1] \\ -\frac{1}{\sqrt{WH(x_i)}}, & x_i = \frac{\pi}{2} \end{cases} \quad (18)$$

Based on Equations (11) and (12), m/h can be expressed as:

$$\frac{m}{h}(x_i) = \frac{WB(x_i)}{WH(x_i)} \quad (19)$$

When the CPCs data after the Suter transformation are given, the values of q/\sqrt{h} , n/\sqrt{h} and m/h can be determined through Equations (17) to (19). The basic principle of mathematical transformation and inverse transformation of the CPCs is shown in Figure 4.

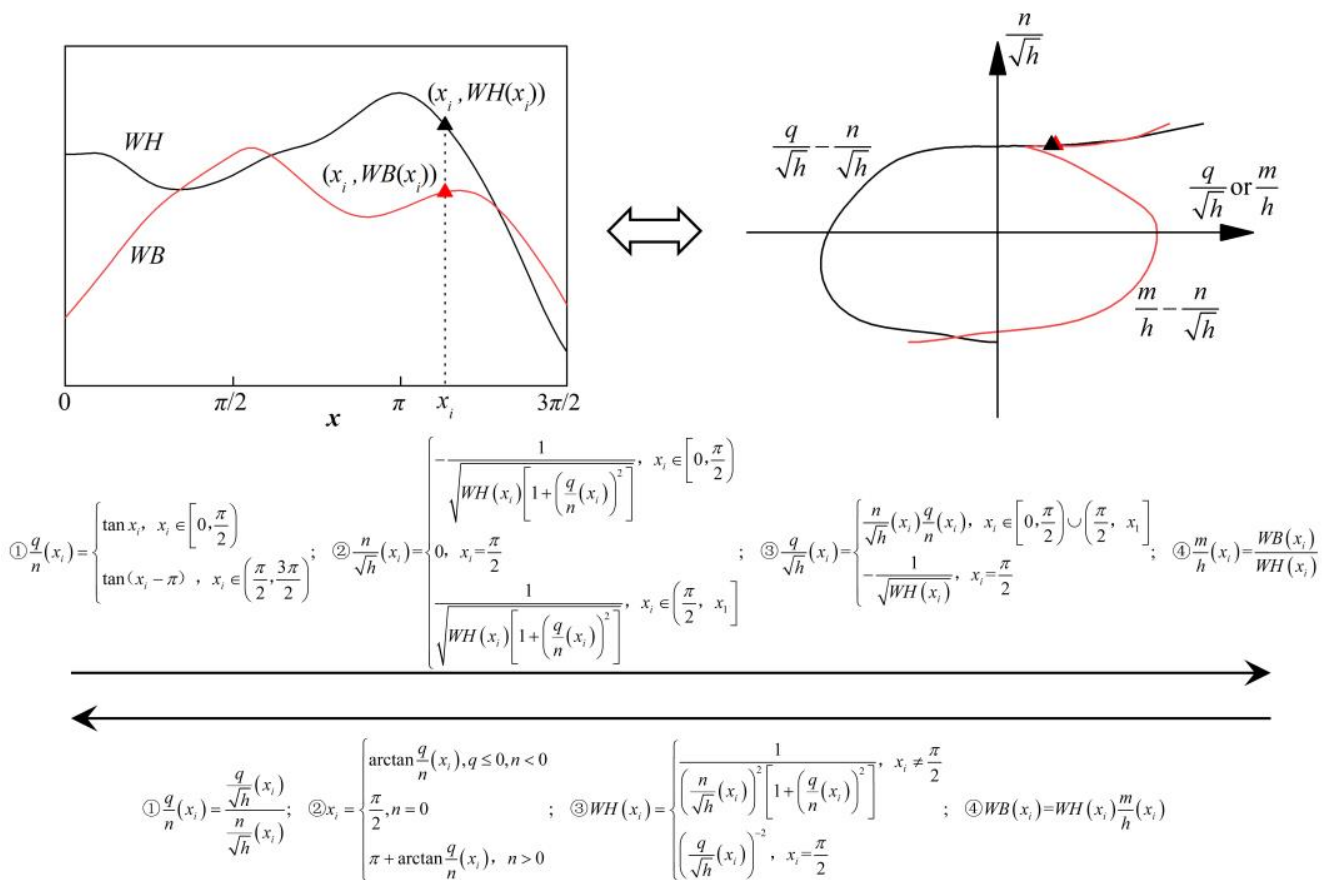


Figure 4. Basic principle of mathematical transformation and inverse transformation of the CPCs.

3.2. COPs Analysis

The generic $q/\sqrt{h} - n/\sqrt{h}$ and $m/h - n/\sqrt{h}$ curves of the pump are presented in Figure 5, showing the distribution of the COPs on the curves, in which four operating regimes are distinguished: turbine, dissipation, normal pump and reverse dissipation [38]. In Figure 5, point A represents the demarcation point of the turbine region and reverse dissipation region, while point C is the demarcation point of the pump region and dissipation region. Their discharges are equal to zero. Point B is the demarcation point of the turbine region and dissipation region, and its speed is equal to zero. Point M represents the runaway point of the pump, whose torque is equal to zero. Point O represents the rated working point of the pump, i.e., the best efficiency point (BEP), and its coordinate value is always (1,1). Moreover, to improve the accuracy of the prediction curves, the COPs would be increased to ensure that there are at least three COPs in each quadrant. Therefore, it is necessary to add some other COPs, e.g., point D in the pump region, which

exists at $(q/\sqrt{h})_D = [(q/\sqrt{h})_C + (q/\sqrt{h})_O]/2 = 0.5$, and point P in the dissipation region, whose included angle with the positive horizontal axis is always 135 degrees, i.e., $(n/\sqrt{h})_P = -(q/\sqrt{h})_P$.

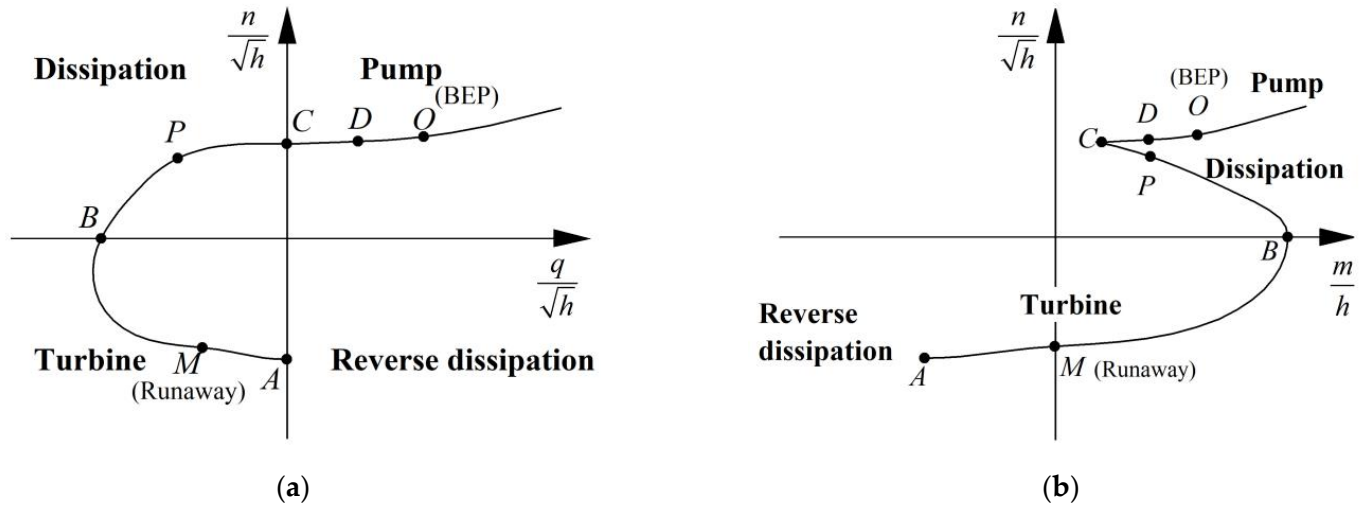


Figure 5. The distribution of the COPs on the characteristic curves after mathematical transformation: (a) $q/\sqrt{h} - n/\sqrt{h}$ curve; (b) $m/h - n/\sqrt{h}$ curve.

The position of the above COPs has a significant impact on the shape of the $q/\sqrt{h} - n/\sqrt{h}$ and $m/h - n/\sqrt{h}$ curves. Indeed, as long as the number of COPs is sufficient and the position coordinates are accurate, the $q/\sqrt{h} - n/\sqrt{h}$ and $m/h - n/\sqrt{h}$ curves of the pump can be determined by combining Equations (9) and (10). On this basis, the CPCs in the form of the Suter transformation ($x-WH$ and $x-WB$ curves) can be drawn by the inverse transformation.

Since the locations of these COPs are related mainly to the specific speed of the pump, for constructing the regression model between the characteristic parameters of each COP and specific speed, i.e., $q/\sqrt{h} = f(n_s)$, $n/\sqrt{h} = f(n_s)$ and $m/h = f(n_s)$, the measured characteristic data of eight centrifugal pumps were collected in Table 1, and the specific speeds of these pumps range from 20 to 90. The specific speed of the pump is defined as:

$$n_s = \frac{N\sqrt{Q}}{H^{3/4}} \tag{20}$$

where n_s represents the specific speed.

For a two-stage pump, the specific speed of the pump shall be calculated with $H/2$ instead of H in Equation (20). For a double-suction pump, the specific speed shall be calculated with $Q/2$ instead of Q [39].

Table 1. Eight centrifugal pumps with different specific speeds.

Serial Number	Specific Speed		Data Source
	US Units	Metric Units (Used in This Paper)	
1	1032	20.00	Ayder [40]
2	1089	21.10	Chen [41]
3	1320	25.60	Brown [42]
4	1496	29.00	Kittredge [43]
5	1555	30.14	Chen [41]
6	1935	37.50	Kittredge [43]
7	3676	71.23	Liu [44]
8	4199	81.37	Chen [41]

Since the dimensionless characteristic parameters are nonlinear functions of n_s , the relationships can be described simply by the regression Model $Y = ax^b$ based on the distribution of data points. To evaluate the fitting quality, the correlation coefficient is defined as follows [45]:

$$R = \frac{\sum_{i=1}^n (y_i - \bar{y})(y'_i - \bar{y}')}{\sqrt{\sum_{i=1}^n (y_i - \bar{y})^2 \sum_{i=1}^n (y'_i - \bar{y}')^2}} \quad (21)$$

where y and y' are the original data and the fitting results, respectively; and \bar{y} and \bar{y}' are the mean values of y and y' , respectively.

3.2.1. Characteristic Parameters of Points A and C

The q/\sqrt{h} values of both points A and C are zero (i.e., the pump discharge is zero). According to Equation (9), $(n/\sqrt{h})_C = \sqrt{1/\zeta_1}$, where ζ_1 is related to the diameter of the impeller outlet, the rated speed and rated head of the pump, i.e., related to the specific speed at the rated operating condition. Figure 6 statistically analyzes the characteristic parameters (n/\sqrt{h} and m/h values) of points A and C according to eight sets of centrifugal pumps with different specific speeds in Table 1. The q/\sqrt{h} value of point C varies within the range of 0.79 to 0.96 with a small variation, and the relationship between $(n/\sqrt{h})_C$ and n_s obtained by fitting the power function $Y = ax^b$ is shown in Figure 6c, with the correlation coefficient R close to 0.87. The n/\sqrt{h} value of point A varies in the range of -1.43 to -1.16 with relatively large variation; therefore, the correlation coefficient R is relatively low and does not exceed 0.60, as shown in Figure 6a. In addition, both $dm/dn > 0$ and $dm/dn < 0$ exist near point C while $dm/dn > 0$ near point A, when the pump is operating near point C, a small oscillation of pump speed will also cause a large change in the pump power and torque, resulting in the correlation coefficient between m/h and n_s of point C lower than that of point A, as shown in Figure 6b,d. The relationships between n_s and the characteristic parameters of points A and C are as follows:

$$\begin{cases} \left(\frac{n}{\sqrt{h}}\right)_A = -0.9107n_s^{0.1058} \\ \frac{q}{\sqrt{h}}_A = 0 \\ \left(\frac{m}{h}\right)_A = -0.0719n_s^{0.8316} \end{cases} \quad (22)$$

$$\begin{cases} \left(\frac{n}{\sqrt{h}}\right)_C = 1.2759n_s^{-0.1101} \\ \frac{q}{\sqrt{h}}_C = 0 \\ \left(\frac{m}{h}\right)_C = 0.0661n_s^{0.4619} \end{cases} \quad (23)$$

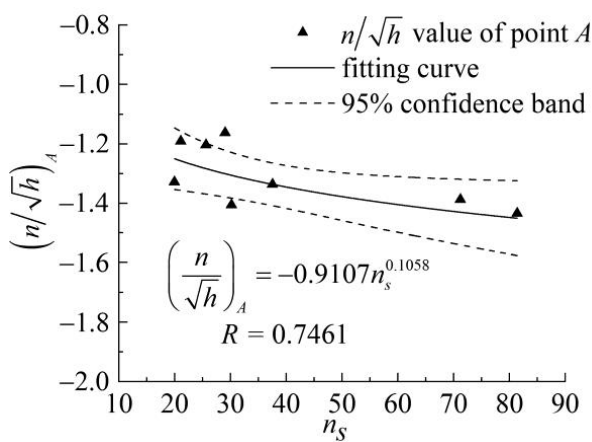
3.2.2. Characteristic Parameters of Points B and M

The n/\sqrt{h} value of point B is zero (i.e., the speed of the pump is zero). At this point, the pump is about to reverse, and small changes in the discharge and shaft torque will also cause large changes in speed. Figure 7 shows the data distribution of the characteristic parameters (q/\sqrt{h} , m/h) of point B. The $(q/\sqrt{h})_B$ value tends to increase gradually with the growth of n_s , while the $(m/h)_B$ value tends to decrease approximately with the growth of n_s . The relationships between $(q/\sqrt{h})_B$ and n_s , $(m/h)_B$ and n_s obtained by the power function fitting are shown in Figure 7a,b, and the correlation coefficients R are 0.9454 and 0.7078, respectively. Point M is the runaway point, and its m/h value is always zero. At this point, the reverse rotational speed of the pump is the largest, and the centrifugal effect of the water flow through the impeller is significant, so the small change in the reverse rotational speed will also lead to a large change in the reverse flow. From Figure 7c, the n/\sqrt{h} value of point M presents less variation, ranging from -1.24 to -1.08 , with a small variation. Therefore, although the correlation coefficient R is less than 0.62, power function fitting can still be used to approximately determine the functional relationship between

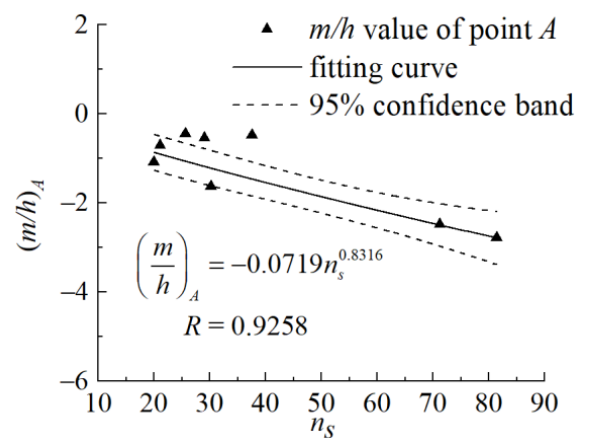
$(n/\sqrt{h})_M$ and n_s . The q/\sqrt{h} value of point M varies from -0.89 to -0.32 with relatively large variation, and the q/\sqrt{h} value shows a gradual decreasing trend with the growth of n_s . The fitted relationship between $(q/\sqrt{h})_M$ and n_s is shown in Figure 7d, and the correlation coefficient R is 0.8655.

$$\begin{cases} \left(\frac{n}{\sqrt{h}}\right)_B = 0 \\ \frac{q}{\sqrt{h}_B} = -3.3672n_s^{-0.3084} \\ \left(\frac{m}{h}\right)_B = 2.6528n_s^{-0.2148} \end{cases} \quad (24)$$

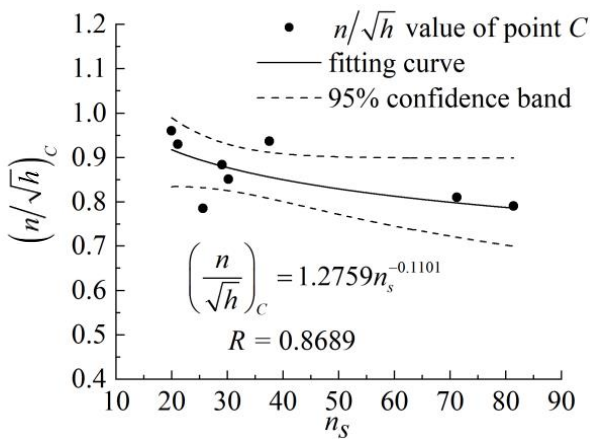
$$\begin{cases} \left(\frac{n}{\sqrt{h}}\right)_M = -0.9500n_s^{0.0581} \\ \frac{q}{\sqrt{h}_M} = -0.2339n_s^{0.2996} \\ \left(\frac{m}{h}\right)_M = 0 \end{cases} \quad (25)$$



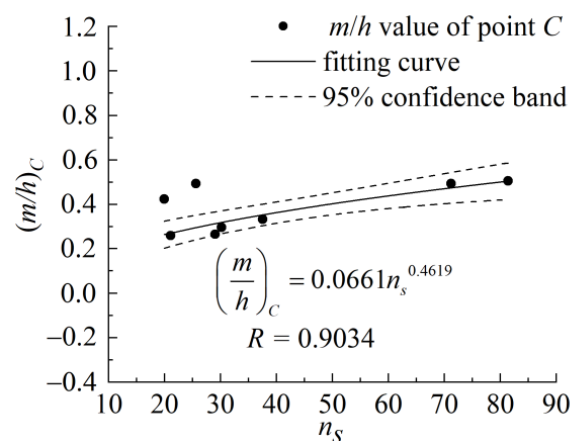
(a)



(b)



(c)



(d)

Figure 6. The relationships between n_s and the characteristic parameters of point A and point C : (a) $(n/\sqrt{h})_A - n_s$; (b) $(m/h)_A - n_s$; (c) $(n/\sqrt{h})_C - n_s$; (d) $(m/h)_C - n_s$.

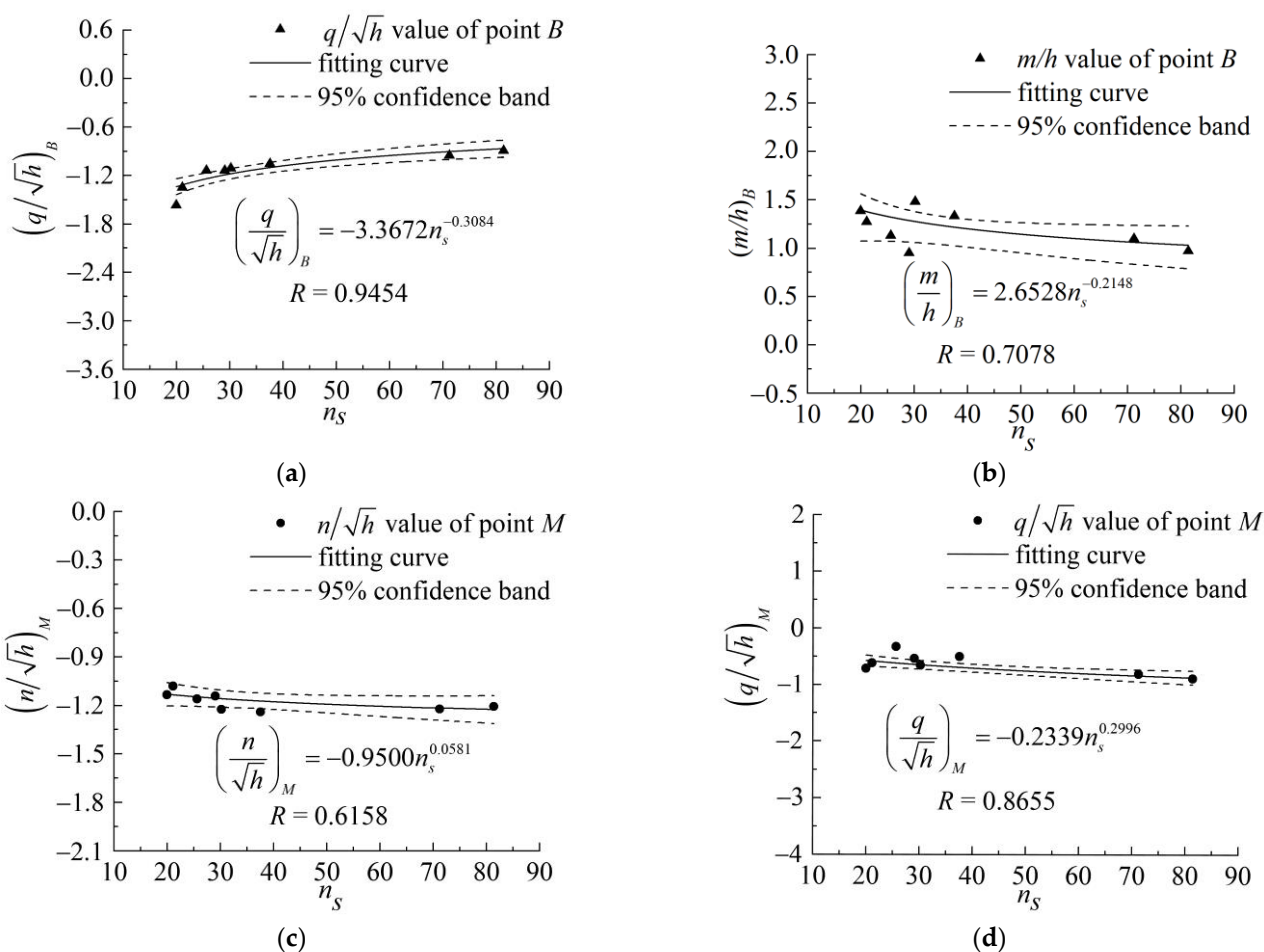


Figure 7. The relationships between n_s and the characteristic parameters of point B and point M : (a) $(q/\sqrt{h})_B - n_s$; (b) $(m/h)_B - n_s$; (c) $(n/\sqrt{h})_M - n_s$; (d) $(q/\sqrt{h})_M - n_s$.

3.2.3. Characteristic Parameters of Points D and P

Points D and P are set as ‘custom’ COPs to satisfy at least three COPs per quadrant, and the statistical data of their corresponding characteristic parameters are shown in Figure 8. The n/\sqrt{h} value of point D is distributed between 0.87 and 0.96, and the range of variation is small. The relationship between $(n/\sqrt{h})_D$ and n_s obtained by the power function fitting is shown in Figure 8a, and the correlation coefficient exceeds 0.86. Additionally, from the statistics of $(n/\sqrt{h})_P - n_s$ and $(q/\sqrt{h})_P - n_s$ shown in Figure 8c,d, respectively, the data points are concentrated above and below the regression model $Y = ax^b$, so the obtained correlation coefficient R is also high, close to 0.87. Figure 8b,e show that the m/h values of points D and P vary greatly, and the distribution of data points is relatively discrete. The correlation coefficients R obtained by the power function fitting are 0.8566 and 0.7622, respectively.

$$\begin{cases} \left(\frac{n}{\sqrt{h}}\right)_D = 1.1261n_s^{-0.0598} \\ \frac{q}{\sqrt{h}_D} = 0.5 \\ \left(\frac{m}{h}\right)_D = 0.2335n_s^{0.2582} \end{cases} \quad (26)$$

$$\begin{cases} \left(\frac{n}{\sqrt{h}}\right)_P = 1.6204n_s^{-0.2519} \\ \left(\frac{q}{\sqrt{h}}\right)_P = -1.6204n_s^{-0.2519} \\ \left(\frac{m}{h}\right)_P = 0.3115n_s^{0.1962} \end{cases} \quad (27)$$

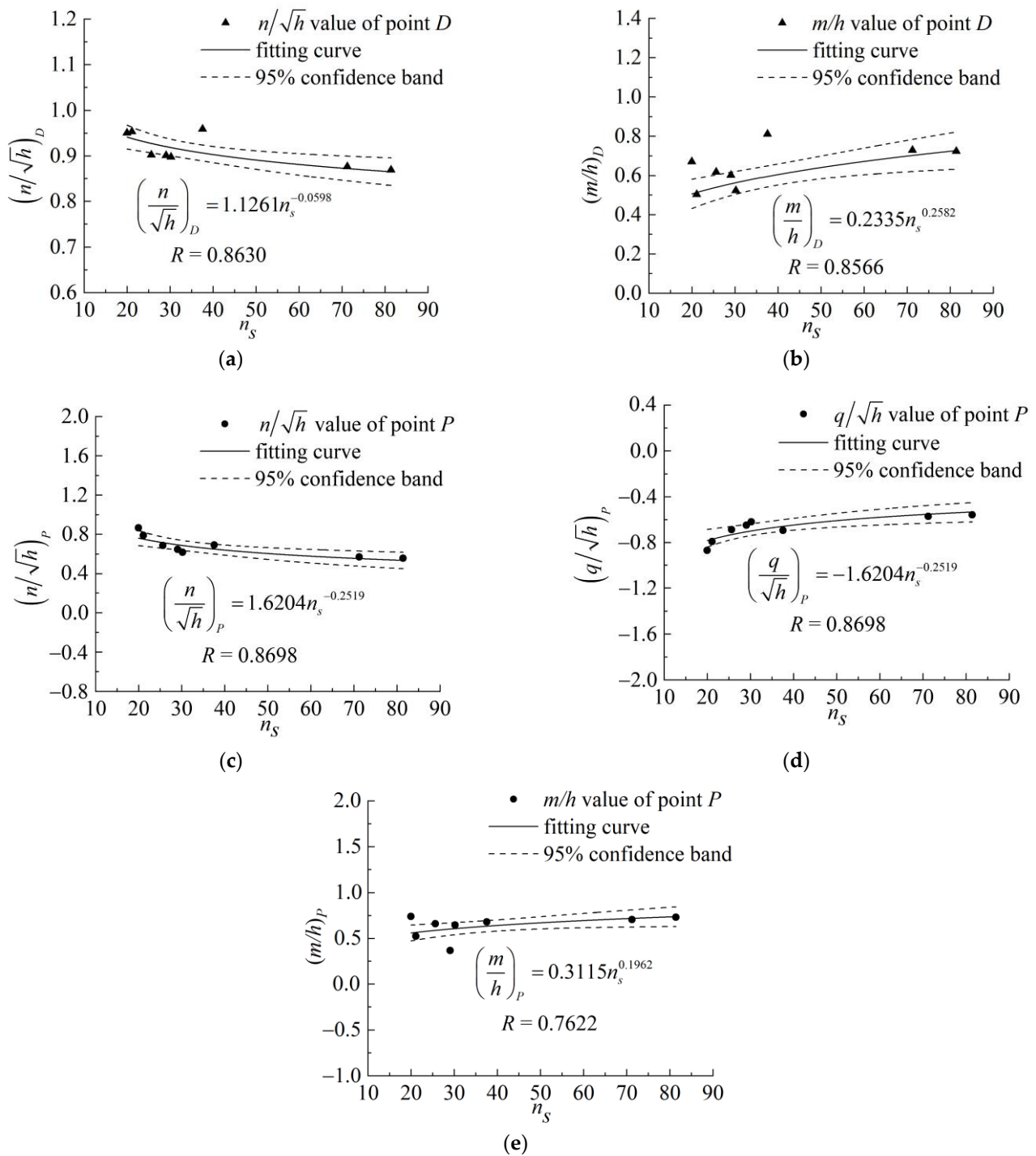


Figure 8. The relationships between n_s and the characteristic parameters of point D and point P : (a) $(n/\sqrt{h})_D - n_s$; (b) $(m/h)_D - n_s$; (c) $(n/\sqrt{h})_P - n_s$; (d) $(q/\sqrt{h})_P - n_s$; (e) $(m/h)_P - n_s$.

4. Model Verification and CPCs Prediction

4.1. Model Verification

To verify the mathematical model proposed in Section 2, the CPC data (x, WH, WB) with $n_s = 24.6$ in the reference [46] are selected as the validation object. The characteristic parameters of COPs on the $q/\sqrt{h} - n/\sqrt{h}$ and $m/h - n/\sqrt{h}$ curves corresponding to $n_s = 24.6$ are obtained by Equations (14) to (19), and their values are shown in Table 2. Then, the characteristic parameters of COPs are substituted into Equation (9), and the values

of undetermined coefficients (ξ_1, ξ_2 , and ξ_3) in the corresponding quadrant are solved by successively selecting each adjacent three COPs. For example, using the adjacent three points *A*, *M*, and *B* to draw the *A-M* segment. In this way, the transformed $q/\sqrt{h} - n/\sqrt{h}$ curve with $n_s = 24.6$ is obtained. Similarly, substituting the characteristic parameters into Equation (10), the values of undetermined coefficients (λ_1, λ_2 and λ_3) are determined, and then the transformed $m/h - n/\sqrt{h}$ curve with $n_s = 24.6$ can be easily obtained. The $q/\sqrt{h} - n/\sqrt{h}$ and $m/h - n/\sqrt{h}$ curves theoretically constructed from the mathematical model in Section 2 are compared with the $q/\sqrt{h} - n/\sqrt{h}$ and $m/h - n/\sqrt{h}$ curves obtained from the measured CPCs after mathematical transformation in Section 3.1, as shown in Figure 9.

Table 2. The characteristic parameters of COPs on the $q/\sqrt{h} - n/\sqrt{h}$ and $m/h - n/\sqrt{h}$ curves corresponding to $n_s = 24.6$.

COPs	$\frac{q}{\sqrt{h}}$	$\frac{n}{\sqrt{h}}$	$\frac{m}{h}$
<i>A</i>	0.0000	-1.2559	-1.0789
<i>M</i>	-0.6526	-1.1520	0.0000
<i>B</i>	-1.2021	0.0000	1.2500
<i>P</i>	-0.7085	0.7085	0.5221
<i>C</i>	0.0000	0.8811	0.3494
<i>D</i>	0.5000	0.9051	0.6592
<i>O</i>	1.0000	1.0000	1.0000

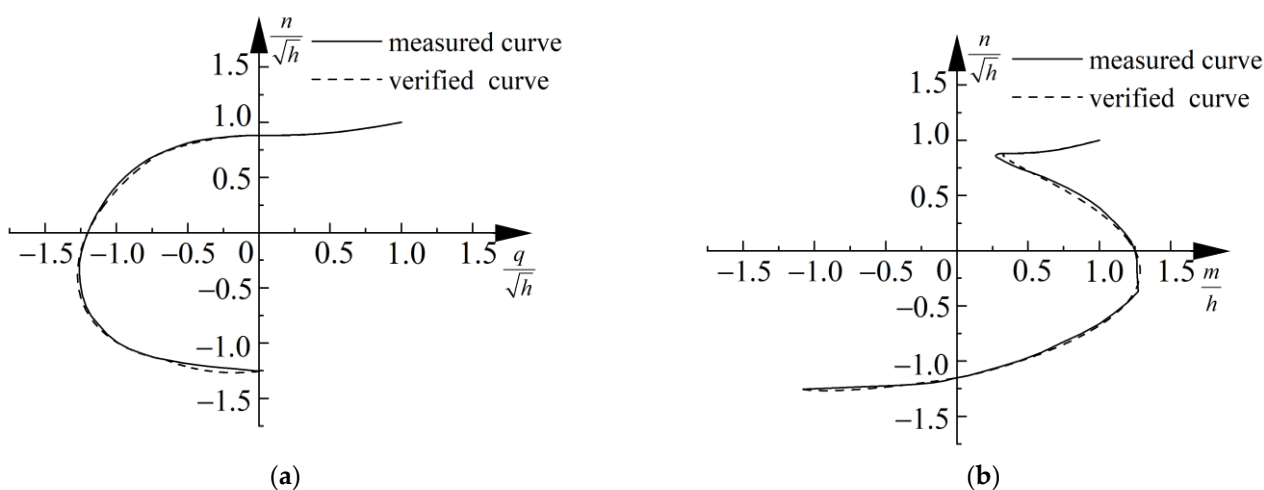


Figure 9. Comparisons of the measured curve and verified curve: (a) $q/\sqrt{h} - n/\sqrt{h}$ curve; (b) $m/h - n/\sqrt{h}$ curve.

As expected, the theoretically constructed $q/\sqrt{h} - n/\sqrt{h}$ and $m/h - n/\sqrt{h}$ curves are highly consistent with the measured $q/\sqrt{h} - n/\sqrt{h}$ and $m/h - n/\sqrt{h}$ curves in each quadrant, also proving that the mathematical model derived in Section 2 to describe the complete characteristic curves of the centrifugal pump is reliable and valid. As long as the characteristic parameters of COPs on the $q/\sqrt{h} - n/\sqrt{h}$ and $m/h - n/\sqrt{h}$ curves are yielded, the CPCs for an arbitrary specific speed can be accurately predicted by combining the established mathematical model. In other words, the engineer needs to test only each characteristic operating condition when conducting the costly and time-consuming model test for CPCs, instead of tediously performing tests on all complex operating conditions such as turbine zone, dissipation zone and reverse dissipation zone, so as to save costs and accelerate the engineering design.

4.2. Prediction Comparison

When the rated parameters of the centrifugal pump (including the rated head, rated discharge and rated speed) are given, the specific speed n_s can be yielded by Equation (20).

Then, according to the relationship model between the characteristic parameters of COPs and n_s established in Section 3.2, the characteristic parameters of COPs can be determined. Substituting these characteristic parameters into the mathematical model in Section 2 (Equations (9) and (10)) and obtaining each of the coefficients to be determined in the model, the $q/\sqrt{h} - n/\sqrt{h}$ and $m/h - n/\sqrt{h}$ curve data are available. Ultimately, the $q/\sqrt{h} - n/\sqrt{h}$ and $m/h - n/\sqrt{h}$ curves can be inverted using the inverse transformation shown in Figure 4 to obtain the CPCs (WH and WB curves). In this paper, $n_s = 24.6$ is selected for prediction and is compared with the measured CPCs. The results are shown in Figures 10 and 11. The CPCs predicted by the theoretical construction are basically in good agreement with the CPCs measured by the pump impeller model test. Nevertheless, due to the complex internal flow regime when the pump operates in the dissipation zone, the statistics of the characteristic parameters of COPs such as points B and C are prone to deviation. However, these deviations are not large. The maximum absolute deviations between the predicted values of WH and WB and their measured values are only 0.06 and 0.15, respectively. Indeed, the accuracy of the CPCs constructed by the prediction method proposed in this paper depends on the statistical accuracy of the characteristic parameters corresponding to the COPs. The higher the statistical accuracy of the characteristic parameters, the higher the accuracy of the CPCs constructed theoretically.

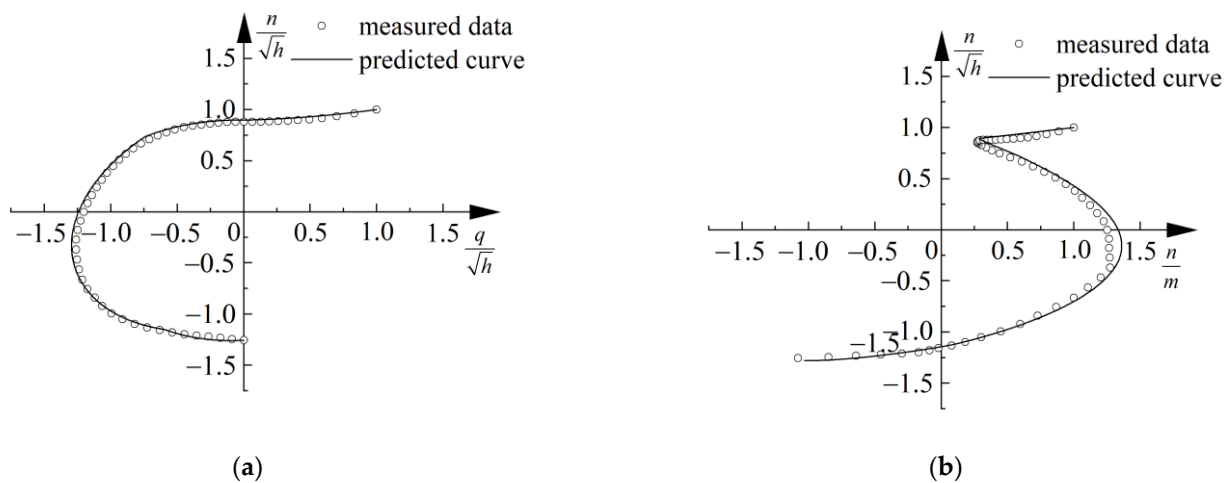


Figure 10. Comparisons of measured curve and predicted curve: (a) comparison of predicted $q/\sqrt{h} - n/\sqrt{h}$ curve and measured data; (b) comparison of predicted $m/h - n/\sqrt{h}$ curve and measured data.

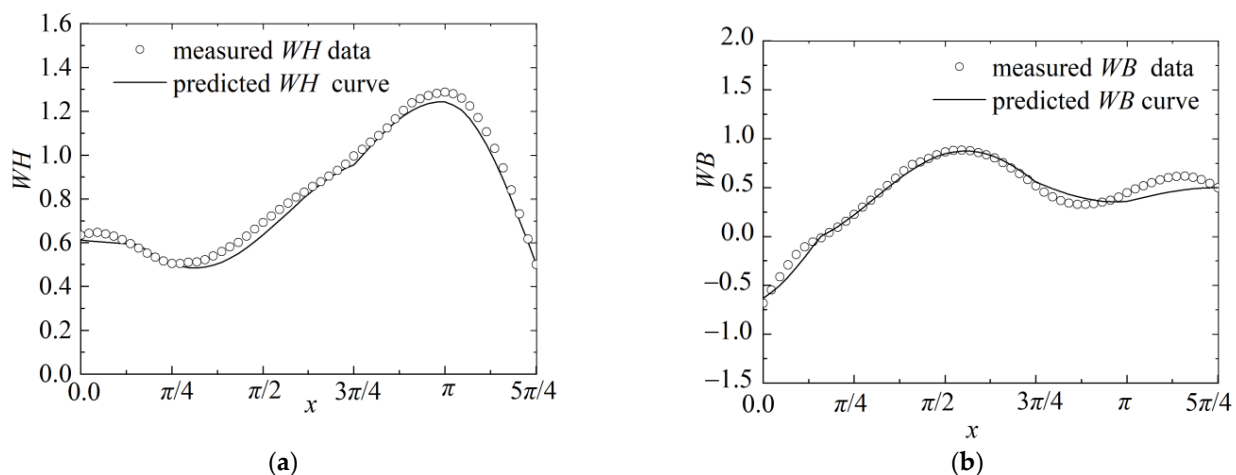


Figure 11. Comparisons of measured complete characteristic curves of pump and predicted complete characteristic data of pump ($0 \leq x \leq 5\pi/4$): (a) comparison of predicted WH curve and measured WH data; (b) comparison of predicted WB curve and measured WB data.

5. Case Study and Discussion

A water delivery pump station in northern China is equipped with four single-stage double-suction centrifugal pumps of the same type, with three working pumps and one reserve pump, and its layout is shown in Figure 12. The reserve pump unit is considered activated with the other three working pumps when the water intake increases the discharge. The rated parameters of a single pump are $Q_r = 1.05 \text{ m}^3/\text{s}$, $H_r = 130 \text{ m}$, $N_r = 993 \text{ rpm}$, $\eta_r = 84.5\%$, and the specific speed of the pump is $n_s = 18.7$, according to Equation (20). The combined pump-motor moment of inertia is $188.75 \text{ kg}\cdot\text{m}^2$. The installation position of the pump is close to the intake pool. Four pumps share one outlet pipe with a total length of 366 m , a diameter of 1400 mm , and an average roughness of 0.014 . The outlet control valve adopts type HQ7x40H-10 slow-closing butterfly valve with a diameter of 1000 mm . The water levels in the upstream intake pool and downstream outlet pool are 1264.65 m and 1395.00 m , respectively.

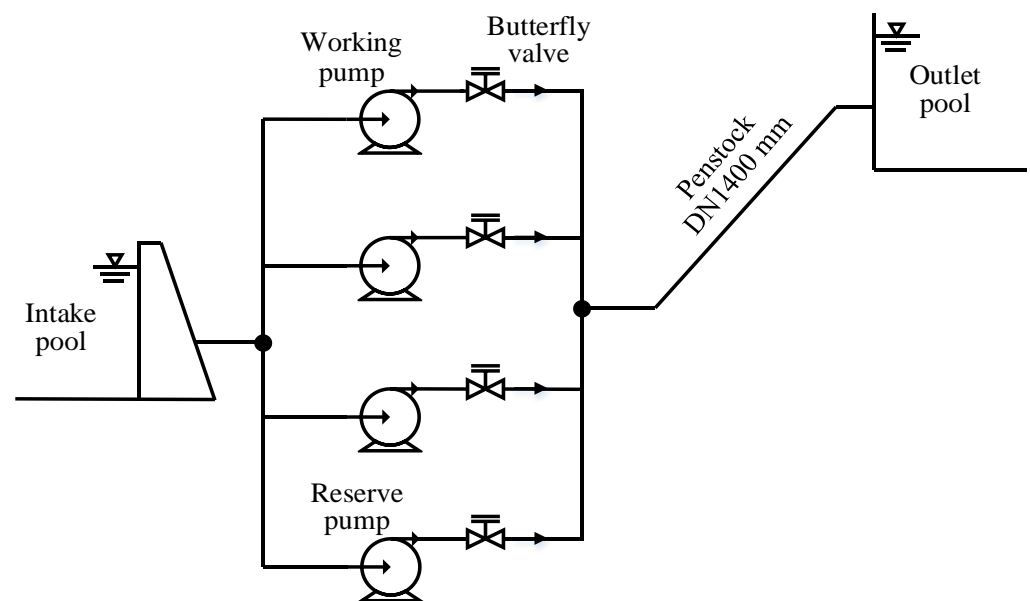


Figure 12. Schematic diagram of pump station layout [39].

Since measured CPCs with $n_s = 18.7$ were lacking, to quantitatively evaluate and verify the reliability of the CPCs prediction method proposed in this paper, numerical simulations of the hydraulic transient process are carried out under the same accidental pump-failure transient conditions using the following CPCs: the predicted CPCs with $n_s = 18.7$ and $n_s = 24.6$ obtained by the prediction method in this paper, the measured CPCs with $n_s = 24.6$, the CPCs with $n_s = 24.6$ obtained by linear interpolation of $n_s = 21.1$ and $n_s = 29.0$ measured data and the measured CPCs with $n_s = 25.6$. Among the transient conditions, the following are included: condition one, in which three working pumps suddenly encounter an accidental power failure and the control valve at the pump outlet fails to close; and condition two, in which three working pumps suddenly encounter an accidental power failure and the control valve at the pump outlet is subjected to a optimized two-stage closing strategy (3 s fast shutdown to 20% opening and 10 s to completely closed). The simulation results of condition one and condition two are shown in Figure 13. The maximum and minimum pressures at the outlet of the control valve and along the pipeline and the maximum relative reverse rotational speed of the pump under these two transient conditions are collected in Table 3.

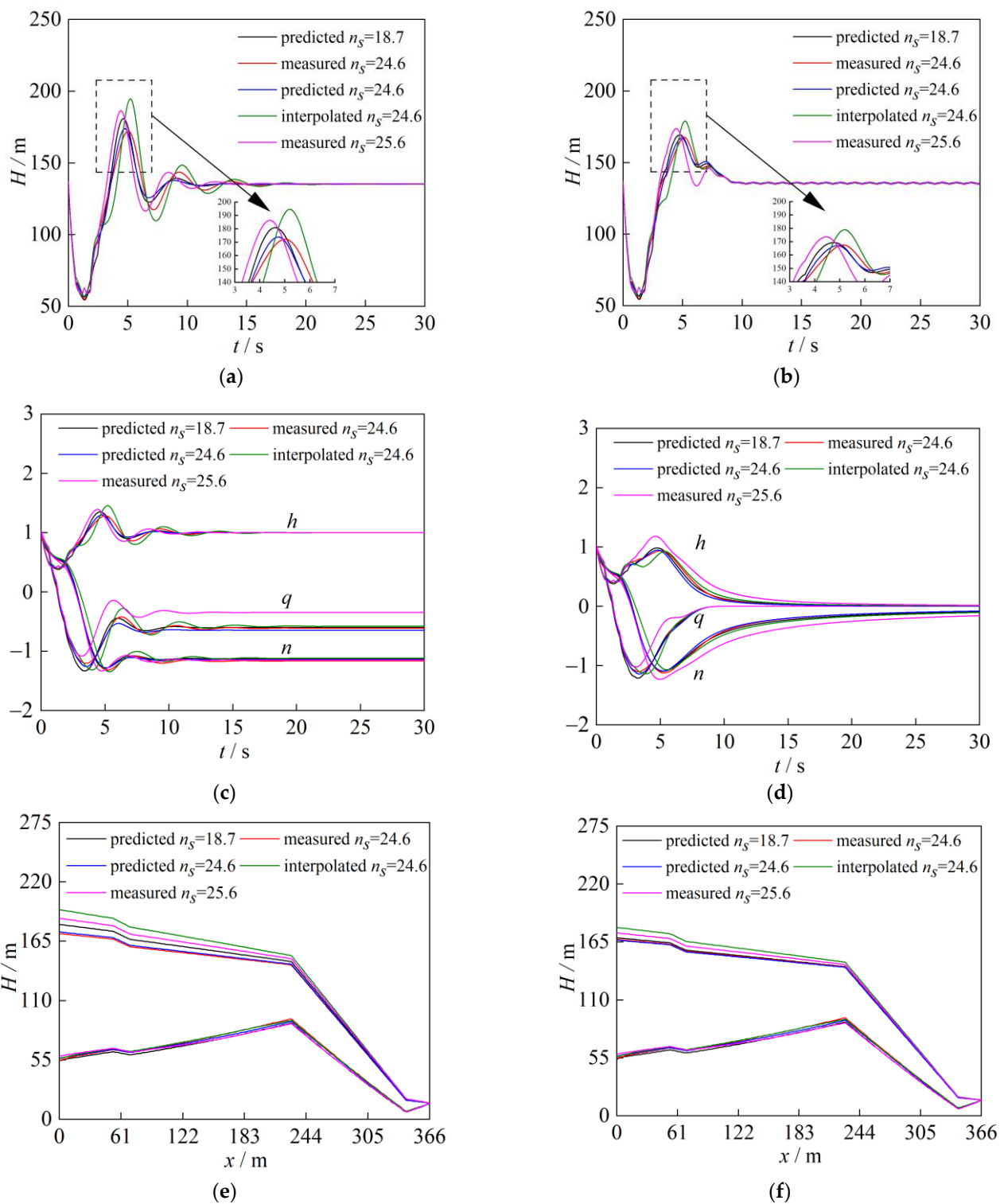


Figure 13. Simulation results of hydraulic transients under valve rejection and valve two-stage closing conditions: (a) variation process of control valve outlet pressure under condition one; (b) variation process of control valve outlet pressure under condition two; (c) variation process of relative speed, discharge and head of the pump under condition one; (d) variation process of relative speed, discharge and head of the pump under condition two; (e) maximum and minimum pressure envelopes along the pipeline under condition one; (f) maximum and minimum pressure envelopes along the pipeline under condition two.

Table 3. Extreme values under valve rejection and valve two-stage closing conditions.

Adopted CPCs	Condition One			Condition Two		
	Max./Min. Head at Control Valve Outlet (m)	Max. Relative Reverse Speed	Max./Min. Head Along Pipeline (m)	Max./Min. Head at Control Valve Outlet (m)	Max. Relative Reverse Speed	Max./Min. Head Along Pipeline (m)
Predicted $n_s = 18.7$	180.87/54.42	−1.29	180.87/6.66	169.33/54.42	−1.10	169.33/6.64
Measured $n_s = 24.6$	172.26/54.95	−1.32	172.26/7.54	167.59/54.95	−1.12	167.59/7.67
Predicted $n_s = 24.6$	173.89/56.81	−1.28	173.89/6.80	167.10/56.81	−1.09	167.10/6.84
Interpolated $n_s = 24.6$	194.58/56.42	−1.34	194.58/7.31	178.94/56.43	−1.07	178.94/7.64
Measured $n_s = 25.6$	186.40/58.82	−1.33	186.40/6.70	173.70/58.86	−1.23	173.70/6.45

From Figure 13 and Table 3, for the condition one, although the specific speeds of $n_s = 24.6$ and $n_s = 25.6$ are close, the simulation results obtained by using the measured CPCs corresponding to the two specific speeds are quite different. The maximum pressure difference at the control valve outlet reaches 14.14 m, and the minimum pressure difference is close to 4 m. The relative deviation of the minimum pressure along the pipeline is more than 11%. The maximum pressure at the control valve outlet obtained by using the linear interpolated CPCs with $n_s = 24.6$ is 22.32 m higher than that obtained by using the measured CPCs with $n_s = 24.6$, and the relative deviation is close to 13%. Moreover, the fluctuation amplitude of the pump head and discharge simulated by interpolated CPCs is larger, which is not conducive to the safe operation of the project. In addition, different from the others, the simulation results obtained by using the predicted CPCs with $n_s = 24.6$ are in good agreement with the simulation results obtained by using the measured CPCs with $n_s = 24.6$, in which the relative deviations of the maximum and minimum pressures at the outlet of the control valve are 0.9% and 3.4%, respectively, and the relative deviation of the maximum reverse rotational speed of the pump is 3.0%. The relative deviation of the minimum pressure along the pipeline is 9.8%, but if the relative deviation of 9.8% is converted into the absolute value, it is only 0.74 m, which is considered acceptable. When the predicted CPCs with $n_s = 18.7$ are used, the maximum and minimum pressures along the pipeline are 180.87 m and 6.66 m, respectively. The maximum relative reverse rotational speed is −1.29, which exceeds 1.2 times of the rated speed of the pump and does not meet the specification requirements.

Similar to condition one, the maximum and minimum pressures at the outlet of the control valve simulated by using the measured CPCs with $n_s = 24.6$ and $n_s = 25.6$ differ greatly, and the differences are 6.11 m and 3.91 m respectively. The relative deviation of the minimum pressure along the pipeline is close to 16%. The maximum pressure at the outlet of the control valve simulated by the interpolated CPCs with $n_s = 24.6$ is 11.35 m higher than that simulated by the measured CPCs with $n_s = 24.6$. However, compared with condition one, since the two-stage closing strategy can alleviate the fluctuation amplitude of the pump head and discharge, the variation process of pump head and discharge simulated by the interpolated CPCs with $n_s = 24.6$ under condition two is basically consistent with the simulation results of the measured CPCs with $n_s = 24.6$. Moreover, for the condition two, the simulation results obtained by using the predicted CPCs and measured CPCs with $n_s = 24.6$ are also in good agreement, in which the relative deviations of the maximum and minimum pressures at the control valve outlet do not exceed 3.4%, and the relative deviation of the maximum reverse rotational speed of the pump does not exceed 2.7%. The deviation of maximum and minimum pressures along the pipeline does not exceed 0.83 m. In addition, the maximum and minimum pressures along the pipeline simulated by using the predicted CPCs with $n_s = 18.7$ under condition two are smaller than that under condition one. The maximum pressure along the pipeline shows the largest difference,

which is 11.54 m. The maximum relative reverse speed is -1.10 , which is less than 1.2 times that of the rated speed of the pump, and meets the specification requirements.

The above analysis shows the following. (1) For some projects, when the measured CPCs are not available, applying the CPCs with an approximate specific speed to simulate the hydraulic transients of the pump station may cause large errors, introducing adverse effects to the safe operation of the project. (2) In addition to applying the CPCs with an approximate specific speed, linear interpolation is often used to obtain the complete characteristic curves of pumps. However, this approach may also produce large errors in the simulation results, causing safety hazards. Furthermore, when the actual specific speed is not within the range of collected pump specific speeds, the corresponding CPCs data cannot be obtained by linear interpolation. (3) The CPCs prediction method proposed in this paper can simulate the common transient processes of pump stations. The simulation results are basically consistent with the simulation results using the measured CPCs, and the error is smaller than the traditional method of using linear interpolation and using the CPCs with an approximate specific speed. It can fully meet the accuracy requirements for the hydraulic transient simulation in the preliminary design of the pump stations, and provide important data support for the design and safe operation of the project.

6. Conclusions

Considering that the traditional prediction method for the CPCs is relatively low in terms of prediction accuracy and ignores the actual operation characteristics of the pump, a novel method considering the inherent operating characteristics of the centrifugal pump is proposed to predict the CPCs, which serves for the design of pump stations. First, a mathematical model describing the complete characteristics of a centrifugal pump is constructed based on the Euler equation and the velocity triangles at the pump impeller. Then, the nonlinear functional relationship between the characteristic parameters corresponding to the COPs on the $q/\sqrt{h} - n/\sqrt{h}$ and $m/h - n/\sqrt{h}$ curves and the specific speed are established based on multiple measured CPCs at various specific speeds. Ultimately, through model verification and a case study, the following conclusions are drawn:

- (1) Under the condition that the characteristic parameters corresponding to all COPs on the $q/\sqrt{h} - n/\sqrt{h}$ and $m/h - n/\sqrt{h}$ curves are known, the CPCs constructed by the mathematical model derived in this paper are in good agreement with the measured CPCs. This proves that the prediction model of the CPCs proposed in this paper is effective. When the characteristic parameters are unknown, by substituting the regression model of the characteristic parameters into the mathematical model describing the CPCs, the CPCs for a given specific speed can be predicted successfully, and the error of WH and WB values is within the acceptable range. Theoretically, the higher the statistical accuracy of characteristic parameters of COPs, the higher the prediction accuracy of the method proposed in this paper.
- (2) The CPCs prediction method proposed in this paper can simulate the common transient processes of pump stations, and the error is smaller than the traditional method of using linear interpolation and using the CPCs with an approximate specific speed. The simulation accuracy of the prediction method can meet the requirements for the hydraulic transient simulation in the preliminary design, and provide important data support for the design and safe operation of the project.

Author Contributions: Conceptualization, W.H. and H.L. (Huokun Li); methodology, H.L. (Huokun Li), W.H. and H.L. (Hongkang Lin); formal analysis, H.L. (Hongkang Lin), H.L. (Huokun Li) and J.L.; data curation, H.L. (Hongkang Lin), M.Z. and X.H.; writing original draft preparation, H.L. (Hongkang Lin); writing review and editing, W.H., H.L. (Huokun Li) and J.M.; supervision, J.M. and J.L.; project administration, W.H.; funding acquisition, W.H., M.Z. and X.H. All authors have read and agreed to the published version of the manuscript.

Funding: This research was funded by the National Natural Science Foundation of China (Grant No. 51909115, 52079061), Natural Science Foundation of Jiangxi, China (Grant No. 20192BAB216038), Open Research Fund of State Key Laboratory of Simulation and Regulation of Water Cycle in River Basin, China Institute of Water Resources and Hydropower Research (Grant No. IWHR-SKL-KF201904), Water Science and Technology Projects of Water Resources Department of Jiangxi Province (Grant No. 202123YBKT04) and 2021 Annual Scientific Research Program of Wanjiashai Water Holding Group Co., Ltd. (Grant No. 2021–30).

Institutional Review Board Statement: Not applicable.

Informed Consent Statement: Not applicable.

Data Availability Statement: Not applicable.

Acknowledgments: Not applicable.

Conflicts of Interest: The authors declare no conflict of interest.

Nomenclature

CPC	complete pump characteristic
COP	characteristic operating point
M	shaft torque, N·m
H_e	theoretical head, m
H	practical head, m
Q	discharge, m ³ /s
K	hydraulic loss coefficient
ω	angular velocity of rotation, rad/s
V_u	peripheral components of the absolute velocity, m/s
r	impeller radius, m
ρ	flow density, kg/m ³
g	gravitational acceleration, m/s ²
V_m	meridional flow velocity, m/s
A	section area, m ²
b	section width, m
U	peripheral velocity, m/s
α_1	absolute flow angle, °
β_2	relative flow angle, °
q	relative discharge
h	relative head
n	relative rotational speed
m	relative torque
N	rotational speed, rpm
n_s	specific speed
WH	head characteristics of pump
WB	torque characteristics of pump
Subscripts	
r	rated condition
$max.$	maximum value
$min.$	maximum value
1	impeller inlet
2	impeller outlet

References

1. Wang, F.J.; Tang, X.L.; Chen, X.; Xiao, R.F.; Yao, Z.F.; Yang, W. A review on flow analysis method for pumping stations. *J. Hydraul. Eng.* **2018**, *49*, 47–61.
2. Dai, C.; Dong, L.; Lin, H.; Zhao, F. A Hydraulic Performance Comparison of Centrifugal Pump Operating in Pump and Turbine Modes. *J. Therm. Sci.* **2020**, *29*, 1594–1605. [[CrossRef](#)]
3. Li, D.; Fu, X.; Zuo, Z.; Wang, H.; Li, Z.; Liu, S.; Wei, X. Investigation methods for analysis of transient phenomena concerning design and operation of hydraulic-machine systems—A review. *Renew. Sustain. Energy Rev.* **2019**, *101*, 26–46. [[CrossRef](#)]

4. Huang, W.; Yang, K.; Guo, X.; Ma, J.; Wang, J.; Li, J. Prediction Method for the Complete Characteristic Curves of a Francis Pump-Turbine. *Water* **2018**, *10*, 205. [[CrossRef](#)]
5. Knapp, R.T. Complete characteristics of centrifugal pumps and their use in the prediction of transient behavior. *Trans. ASME* **1937**, *59*, 683–689.
6. Huang, B.; Wu, P.; Liu, X.S.; Feng, X.D.; Yang, S.; Wu, D.Z. Four-quadrant Full Characteristic Model Test of the ACP100 Reactor Coolant Pump. *Fluid Mach.* **2020**, *48*, 8–11.
7. Shukla, S.N.; Kshirsagar, J.T. Numerical Experiments on a Centrifugal Pump. In Proceedings of the ASME 2002 Joint U.S.-European Fluids Engineering Division Conference, Montreal, QC, Canada, 14–18 July 2002; pp. 709–719.
8. Donsky, B. Complete Pump Characteristics and the Effects of Specific Speeds on Hydraulic Transients. *J. Fluids Eng.* **1961**, *83*, 685. [[CrossRef](#)]
9. Yang, Y.S.; Dong, R.; Jing, T. Influence of Full Characteristic Curve on Pump-off Water Hammer and Its Protection. *China Water Wastewater* **2010**, *26*, 63–66.
10. Marchal, M.; Flesch, G.; Suter, P. The calculation of waterhammer problems by means of the digital computer. In Proceedings of the International Symposium on Waterhammer in Pumped Storage Projects ASME, Chicago, IL, USA, 7–11 November 1965; pp. 168–180.
11. Zhang, C.; Peng, T.; Zhou, J.; Ji, J.; Wang, X. An improved autoencoder and partial least squares regression-based extreme learning machine model for pump turbine characteristics. *Appl. Sci.* **2019**, *9*, 3987. [[CrossRef](#)]
12. Izquierdo, J.; Montalvo, I.; Pérez-García, R.; Ayala-Cabrera, D. Multi-agent simulation of hydraulic transient equations in pressurized systems. *J. Comput. Civ. Eng.* **2016**, *30*, 04015071. [[CrossRef](#)]
13. Zhu, M.L.; Zhang, X.H.; Zhang, Y.H.; Wang, T. Study on prediction model of complete characteristic curves of centrifugal pumps. *J. Northwest Sci-Tech Univ. Agric. For. Nat. Sci. Ed.* **2006**, *4*, 143–146.
14. Hu, X.Y.; Yu, B.; Guo, J.; Wang, S.K. Visualization for predictable model of complete characteristic curve of pump. *Fluid Mach.* **2012**, *3*, 37–39.
15. Lima, G.M.; Luvizotto Júnior, E. Method to estimate complete curves of hydraulic pumps through the polymorphism of existing curves. *J. Hydraul. Eng.* **2017**, *143*, 04017017. [[CrossRef](#)]
16. Wan, W.; Huang, W. Investigation on complete characteristics and hydraulic transient of centrifugal pump. *J. Mech. Sci. Technol.* **2011**, *25*, 2583–2590. [[CrossRef](#)]
17. Liu, G.L.; Jiang, J.; Fu, X.Q. Predicting complete characteristics of pumps by using BP neural network. *J. Wuhan Univ. Hydraul. Electr. Eng.* **2000**, *2*, 37–39.
18. Lu, W.; Li, L.G. Drawing the all-character curve of water pump on BP neural network. *Ind. Control. Comput.* **2001**, *14*, 18–20.
19. Liu, Z.F. GARBF Network Method to Predict the Complete Characteristic Curve of Pump. Master's Thesis, Chang'an University, Xi'an, China, 2011.
20. Han, W.; Nan, L.; Su, M.; Chen, Y.; Li, R.; Zhang, X. Research on the prediction method of centrifugal pump performance based on a double hidden layer BP neural network. *Energies* **2019**, *12*, 2709. [[CrossRef](#)]
21. Huang, S.; Qiu, G.; Su, X.; Chen, J.; Zou, W. Performance prediction of a centrifugal pump as turbine using rotor-volute matching principle. *Renew. Energy* **2017**, *108*, 64–71. [[CrossRef](#)]
22. Wu, Q.; Wang, X.; Shen, Q. Research on dynamic modeling and simulation of axial-flow pumping system based on RBF neural network. *Neurocomputing* **2016**, *186*, 200–206. [[CrossRef](#)]
23. Höller, S.; Benigni, H.; Jaberg, H. Investigation of the 4-Quadrant behaviour of a mixed flow diffuser pump with CFD-methods and test rig evaluation. *IOP Conf. Ser. Earth Environ. Sci.* **2016**, *49*, 032018. [[CrossRef](#)]
24. Gros, L.; Couzinet, A.; Pierrat, D.; Landry, L. Complete pump characteristics and 4-quadrant representation investigated by experimental and numerical approaches. In Proceedings of the ASME-JSME-KSME 2011 Joint Fluids Engineering Conference, Hamamatsu, Japan, 24–29 July 2011; pp. 359–368.
25. Wang, L.; Li, M.; Wang, F.J.; Wang, J.B.; Yao, C.G.; Yu, Y.S. Study on three-dimensional internal characteristics method of Suter curves for double-suction centrifugal pump. *J. Hydraul. Eng.* **2017**, *48*, 113–122.
26. Muttalli, R.S.; Agrawal, S.; Warudkar, H. CFD simulation of centrifugal pump impeller using ANSYS-CFX. *Intern. J. Innov. Res. Sci. Eng. Technol.* **2014**, *3*, 15553–15561. [[CrossRef](#)]
27. Frosina, E.; Buono, D.; Senatore, A. A performance prediction method for pumps as turbines (PAT) using a computational fluid dynamics (CFD) modeling approach. *Energies* **2017**, *10*, 103. [[CrossRef](#)]
28. Chang, J.S. *Transients of Hydraulic Machine Installations*; Higher Education Press: Beijing, China, 2005.
29. Zhang, Y.L.; Zhu, Z.C.; Dou, H.S.; Cui, B.L. A Generalized Euler Equation to Predict Theoretical Head of Turbomachinery. *Int. J. Rotating Mach.* **2015**, *42*, 26–38. [[CrossRef](#)]
30. El-Naggar, M.A. A one-dimensional flow analysis for the prediction of centrifugal pump performance characteristics. *Int. J. Rotating Mach.* **2013**, *2013*, 473512. [[CrossRef](#)]
31. Olimstad, G.; Nielsen, T.; Børresen, B. Dependency on runner geometry for reversible-pump turbine characteristics in turbine mode of operation. *J. Fluids Eng.* **2012**, *134*, 121102. [[CrossRef](#)]
32. Tanaka, T.; Liu, C. An Investigation on Velocity Triangle Applied to Fluid Particle at Rotating Flow Passage of Impeller Blade in Centrifugal Pump. In Proceedings of the ASME 7th Biennial Conference on Engineering Systems Design and Analysis, Manchester, UK, 19–22 July 2004; pp. 433–442.

33. Nicolet, C. Hydroacoustic Modelling and Numerical Simulation of Unsteady Operation of Hydroelectric Systems. Ph.D. Thesis, École Polytechnique Fédérale de Lausanne (EPFL), Lausanne, Switzerland, 2007.
34. Xu, H.Q.; Lu, L.; Tan, D.Q.; Li, T.Y. Specific speed of pump and unit parameter selection. In Proceedings of the 20th China Hydropower Equipment Symposium, Chengdu, China, 15–17 October 2015.
35. Yang, K.L. *Hydraulic Transients and Regulation in Power Station and Pump Station*; China Water Conservancy and Hydropower Press: Beijing, China, 2000.
36. Matteo, L.; Cerru, F.; Dazin, A.; Tauveron, N. Investigation of the pump, dissipation and inverse turbine operating modes using the CATHARE-3 one-dimensional rotodynamic pump model. In Proceedings of the ASME-JSME-KSME 2019 8th Joint Fluids Engineering Conference, San Francisco, CA, USA, 28 July–1 August 2019.
37. Wu, D.Z.; Xu, B.J.; Li, Z.F.; Wang, L.Q. Numerical Simulation On Internal Flow Of Centrifugal Pump During Transient Operation. *J. Eng. Thermophys.* **2009**, 781–783.
38. Chang, J.S. Analysis of Whole Characteristic Curve and Their Special Condition Points in Mixed-flow Pump-turbine. *J. Beijing Agric. Eng. Univ.* **1995**, 015, 77–83.
39. Huang, W.; Kang, Q.; Li, S.S.; Zhu, Y.X.; Yan, F.; Li, J.Z. Analysis of the effect of valve characteristics on hydraulic transition process of pumping station. *South-to-North Water Transf. Water Sci. Technol.* **2019**, 17, 6.
40. Ayder, E.; Ilikan, A.N.; Sen, M.; Ozgur, C.; Kavurmacioglu, L.; Kirkkopru, K. Experimental investigation of the complete characteristics of rotodynamic pumps. In Proceedings of the ASME 2009 Fluids Engineering Division Summer Meeting, Vail, CO, USA, 2–6 August 2009; pp. 35–40.
41. Chen, N.X. *Simulation and Control of Hydraulic Transients in Hydropower Projects*; China Water Power Press: Beijing, China, 2005.
42. Brown, R.J.; Rogers, D.C. Development of Pump Characteristics from Field Tests. *J. Mech. Des.* **1980**, 102, 807–817. [[CrossRef](#)]
43. Kittredge, C.; Princeton, N. Hydraulic transients in centrifugal pump systems. *Trans. ASME* **1956**, 78, 1307–1321.
44. Liu, G.L.; Guo, M.H. Computer simulation of universal complete pump characteristics. *J. Hydraul. Eng.* **1998**, 8, 2–8. [[CrossRef](#)]
45. Xie, A.; Li, D.H. *Probability and Statistics*; Tsinghua University Press: Beijing, China, 2012.
46. Wylie, E.B.; Streeter, V.L. *Fluid Transients*; McGraw-Hill International Book Co.: New York, NY, USA, 1978.